2019

Breaks, trends and the attribution of climate change: a time-series analysis

2019, Volume 42, Issue 1, 1-31 / ISSN 2304-4306

E C O N O M Í A

revistas.pucp.edu.pe/economia

www.fondoeditorial.pucp.edu.pe

Breaks, Trends and the Attribution of Climate Change: A Time-Series Analysis

Francisco Estrada[a, b], Pierre Perron[c,*]

[a]Centro de Ciencias de la Atmósfera, Universidad Nacional Autónoma de México, Ciudad Universitaria, Circuito Exterior, 0451 Mexico, DF, Mexico

[b]Institute for Environmental Studies, Vrije Universiteit, Amsterdam, Netherlands
✉ feporrua@atmosfera.unam.mx

[c]Department of Economics, Boston University, 270 Bay State Rd., Boston, MA, 02215, USA
✉ perron@bu.edu * Corresponding author

Abstract

Climate change detection and attribution have been the subject of intense research and debate over at least four decades. However, direct attribution of climate change to anthropogenic activities using observed climate and forcing variables through statistical methods has remained elusive, partly caused by difficulties to correctly identify the time-series properties of these variables and by the limited availability of methods to relate nonstationary variables. This paper provides strong evidence concerning the direct attribution of observed climate change to anthropogenic greenhouse gases emissions by first investigating the univariate time-series properties of observed global and hemispheric temperatures and forcing variables and then by proposing statistically adequate multivariate models. The results show that there is a clear anthropogenic fingerprint on both global and hemispheric temperatures. The signal of the well-mixed Greenhouse Gases (GHG) forcing in all temperature series is very clear and accounts for most of their secular movements since the beginning of observations. Both temperature and forcing variables are characterized by piecewise linear trends with abrupt changes in their slopes estimated to occur at different dates. Nevertheless, their long-term movements are so closely related that the observed temperature and forcing trends cancel out. The warming experimented during the last century was mainly due to the increase in GHG which was partially offset by the effect of tropospheric aerosols. Other forcing sources, such as solar, are shown to only contribute to (shorter-term) variations around the GHG forcing trend.

Article History: Received: 19 February 2019 / Revised: 12 April 2019 / Accepted: 12 May 2019
Keywords: Segmented trends; Temperatures; Greenhouse gases; Radiative forcings; Anthropogenic influence
JEL Classification: C32

Acknowledgements

We thank Gabriel Rodríguez and a referee for useful comments.

https://doi.org/10.18800/economia.201901.001

1. Introduction

The scientific literature on climate change shows sound direct and indirect scientific evidence about the warming of the climate system during the 20th century and of its anthropogenic component. A considerable amount of the available attribution studies is based on model predictions about how the world would be with and without anthropogenic interventions with the climate system. However, direct attribution of climate change to anthropogenic activities using observed climate and forcing variables through statistical methods has remained contentious. Examples of the application of statistical techniques to address the attribution of climate change are Stern and Kaufmann (1997a,b), Kaufmann et al. (2006a,b), Tol and De Vos (1993, 1998), Hui and Rodríguez (2005), among others, who showed how the possible presence of stochastic trends in temperature and forcing series could be interpreted. Since then, important advances have been proposed in testing for unit roots, which have significantly changed econometric modeling (see Perron, 2006 for a review) and are useful to address the detection and attribution of climate change (Gay-Garcia et al., 2009; Estrada et al., 2010; Estrada et al., 2013a; Mills, 2010a,b; Gil-Alana, 2008). This literature has shown that the assumption on which these earlier attribution studies are based on (i.e., temperatures and forcing variables being integrated processes) was not soundly tested and that there are strong reasons from both statistical and climate physics perspectives for questioning this assumption (Estrada et al., 2010; Gay-Garcia et al., 2009; see also Triacca, 2001).

This paper first investigates the time-series properties of temperatures and forcing variables using recent econometric techniques to determine what type of data generating process best describes them. Establishing these properties then allows testing for the existence of long-term relationships between temperatures and forcing variables. It is shown that both temperature and different combinations of the radiative forcing variables can be best represented as trend stationary processes with a one-time structural change in the slope of the trend functions occurring at different dates and of diverse magnitudes. In spite of these differences, the multivariate models indicate that the long-term movements of all these variables are so closely related that the observed temperature and forcing trends cancel out, producing stationary residuals. The results show a clear anthropogenic fingerprint on both global and hemispheric temperatures. In particular, well-mixed Greenhouse Gases (GHG) is the variable which contributes the most to the secular movement of the total observed radiative forcing. Its signal is clearly imprinted in all temperature series and accounts for most of their long-term movement since the beginning of observations.

Our analysis suggests a break in the slope of the trend function of the first principal component of the forcing variables. The post-break trend slope is twice the value of the pre-break slope value and the resulting post-break trend slopes of global, northern and southern hemispheres temperatures are up to 7, 9 and 10 times larger than their pre-break slope values, respectively. The contribution of the different forcing variables is also estimated and it is shown that the warming experimented during the last century was mainly due to the increase in GHG, which was partially offset by the effect of tropospheric aerosols. Other forcing sources, such as solar,

mainly contribute to shorter-term variations around the GHG forcing trend and are shown to play no role on the short-run dynamics of temperature series, at least in annual time-scales.

This manuscript was the starting point for some ideas that were developed further and published later, with different methods and newer data. The objective of this contribution is to show some extensions that were never explored further in the context of the research that the authors have published elsewhere. In particular the results presented here show robustness to different datasets and methods. See, in particular, Estrada et al. (2013a,b, 2017), Estrada and Perron (2017, 2019). A review of the statistical methods used can be found in Estrada and Perron (2014).

The paper is structured as follows. Section 2 presents a univariate analysis of the time series properties of the various variables used, both temperatures and radiative forcings. Section 3 establishes the fact that temperatures and forcings share a common breaking trend. Section 4 provides a brief analysis of the short-run dynamics and results from Granger causality tests. A time series model for global and hemispheric temperatures is presented in Section 5. In Section 6, our selected model is shown to provide improved forecasts compared to that of Kaufmann et al. (2006a), which assumes integrated series that are cointegrated. Brief concluding remarks are offered in Section 7.

2. Univariate Analysis of the Time-Series Properties

The time-series properties of annual global and hemispheric temperatures from both the Climatic Research Unit's HadCRUT3 (Brohan et al., 2006) and the NASA database (Hansen et al., 2010) are analyzed (henceforth, we simply use HadCRUT3 and NASA when referring to the respective datasets). The HadCRUT3 spans the period 1850-2010 while NASA covers only 1880-2010. The series are presented in Figure 1. Below, we show strong evidence for trend-stationarity when using unit root tests that allow for a break in the trend function (Kim and Perron, 2009; Perron, 1997, 1989). These results are broadly similar to those of Gay-Garcia et al. (2009) and Estrada et al. (2013a), except that we provide evidence for the presence of two breaks in the slope of the trend function of the southern hemisphere's temperature. We also show these breaks to also be present in the radiative forcing produced by well-mixed GHG.

The standard Augmented Dickey-Fuller unit root test (ADF, Dickey and Fuller, 1979; Said and Dickey, 1984) applied to global and hemispheric temperatures seems to provide strong evidence for a unit root; see Table 1; other most recent unit root tests proposed by Ng and Perron (2001) also suggest the same results. However, as shown by Perron (1989) these results can be misleading if there are breaks in the trend function of the time-series. Figure 1 suggests the presence of structural breaks in the slopes of the trends of all temperatures series. Hence, the results in Table 1 could be misleading. To test for the existence of these breaks, we applied the testing procedure of Perron and Yabu (2009) which is valid whether the noise component is I(1) or I(0) and thus circumvents the problem of pretesting for a unit root usually needed to apply structural change tests. From the results reported in Table 2, the stability of the slope parameter of the trend function for all temperature series is rejected at the 1 % significance level, providing

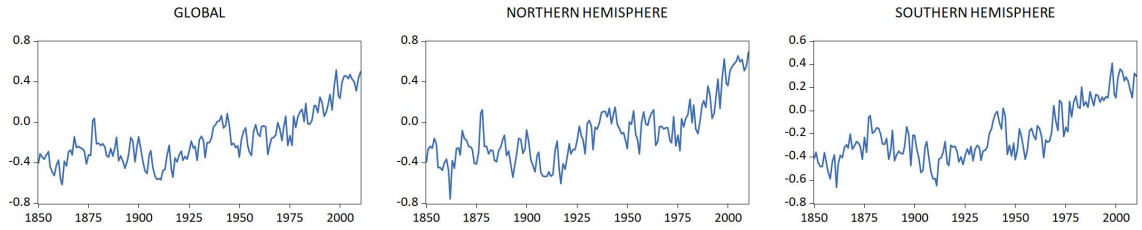

(a) HadCRUT3 (sample 1850-2010)

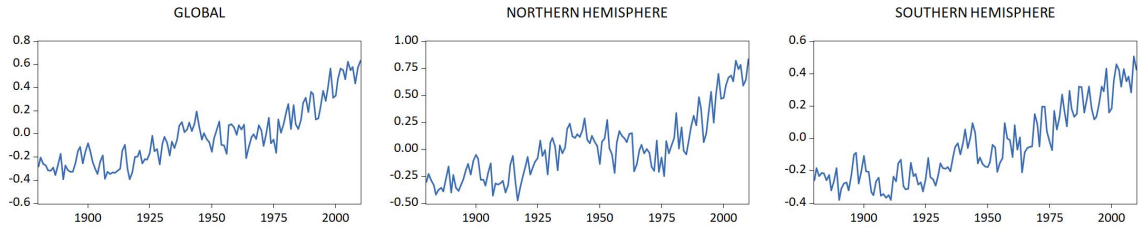

(b) NASA (sample 1880-2010)

Figure 1. Time series plot of the global and hemispheric temperatures series from the HadCRUT3 and NASA datasets.

strong arguments for the need of unit root tests that allow for a one-time break in the trend function.

Perron (1989) first suggested unit root tests in the presence of structural breaks in the trend. Several methods have been developed to extend his original tests to the case of an unknown break date; e.g. Perron (1997), Zivot and Andrews (1992) and Perron and Rodríguez (2003). For these tests the possibility of a break is only allowed under the alternative hypothesis (stationary noise component) and not under the null (integrated noise component). The literature has shown that the Zivot and Andrews (1992) test and some of the tests proposed in Perron (1997) can reject the null hypothesis of a unit root if there is a large break in the slope of the trend function when a unit root noise component is actually present (see Vogelsang and Perron, 1998; Kim and Perron, 2009). To avoid this problem, Kim and Perron (2009) present new unit root testing procedures based on the original test of Perron (1989) that allow for a break in the trend function both under the null and alternative hypotheses and that include a pretest for the existence of a break using the Perron and Yabu (2009) test. If this pre-test rejects, the limit distribution of the unit root test is then the same as if the break date was known (see Perron, 1989; Perron and Vogelsang, 1993). This is very advantageous since when a break is present the test has much greater power.

2.1. Results for Observed Global and Hemispheric Temperatures

We apply the Kim and Perron (2009) and the version of the Perron (1997) tests based on selecting the break date by minimizing the t-statitistic of the change in slope, which is immune to the size problem alluded to above. The "changing growth" model is assumed for global and hemispheric temperature series given that global warming would imply a change in the rate of increase of these variables, as was also proposed in Gay-Garcia et al. (2009) and Estrada et al.

Table 1

Standard Augmented Dickey-Fuller test applied to temperature series.

Series	ADF test statistic
Global (NASA)	-1.49
Global (HadCRUT3)	-2.30
NH (NASA)	-1.75
NH (HadCRUT3)	-2.40
SH (NASA)	-2.92
SH (HadCRUT3)	-2.80

Note: The AIC information criterion was used to select the lag length, and the deterministic regressors were a constant and a trend. None of the statistics are significant at the 5 % level (critical value: -3.41).

Table 2

Perron and Yabu (2009) tests for structural changes in the trend function for time series with an integrated or stationary noise component.

Series	Exp-Wald statistic
Global (NASA)	5.20[a]
Global (HadCRUT3)	4.36[a]
NH (NASA)	4.04[a]
NH (HadCRUT3)	4.93[a]
SH (NASA)	5.14[a]
SH (HadCRUT3)	5.77[a]

Note: a, b, c denote statistical significance at the 1 %, 5 % and 10 %, respectively.

(2013a). As shown in Table 3, the results provide quite clear evidence for trend-stationarity once a break in the slope of the trend is allowed. For all time series and with both tests, the null hypothesis of a unit root is rejected at the 1 % significance level in favor of a trend stationary process with one-time change in the rate of growth. The changes have occurred at different times in the global and hemispheric temperatures and consisted in abrupt increases of different magnitudes in the rate of warming.

It is important to note that in the case of global and northern hemisphere temperatures the estimates of the break dates are quite similar for both the HadCRUT3 and the NASA time series: 1971 and 1978 and 1984 and 1985 for the global and northern hemisphere temperatures from the HadCRUT3 and NASA, respectively. As revealed by the results of applying the methodology of Perron and Zhu (2005), when considering a 95 % confidence interval one cannot consider the estimates of the break dates from these databases to be statistically different (Table 4). It is also worth noting that the break dates from global and northern hemisphere temperatures are not statistically different, regardless of which database is used. These results are also congruent with those shown in Gay-Garcia et al. (2009). Nevertheless, the estimates of the break date in the southern hemisphere temperature are quite different, and depend on the database selected. The results obtained using the NASA dataset are very similar to those in Gay-Garcia et al. (2009), where the break in the trend function is estimated to occur at the beginning of the 20th century.

Table 3

Tests for a unit root with a one-time break in the trend function, HadCRUT3 (C) and NASA (N) data.

Series	T_b	k	$\hat{\mu}$	$t_{\hat{\mu}}$	$\hat{\beta}$	$t_{\hat{\beta}}$	$\hat{\gamma}$	$t_{\hat{\gamma}}$	$\hat{\alpha}$	$t_{\hat{\alpha}}$	$S(\hat{e})$	$t_\alpha(\hat{\lambda}_{tr}^{AO})$
G_C	1971	0	-0.40	-18.09	0.0022	7.45	0.0136	10.17	0.59	-6.37[a]	0.126	-5.61[a]
NH_C	1984	0	-0.40	-15.37	0.0030	9.27	0.0243	9.45	0.58	-6.46[a]	0.154	-5.91[a]
SH_C	1955	0	-0.38	-17.03	0.0011	3.12	0.0099	10.26	0.55	-6.86[a]	0.122	-6.26[a]
G_N	1978	0	-0.32	-16.58	0.0039	12.15	0.0129	9.04	0.40	-7.45[a]	0.091	-6.40[a]
NH_N	1985	0	-0.31	-11.81	0.0042	10.02	0.0235	9.00	0.46	-6.90[a]	0.124	-5.57[a]
SH_N	1923	0	-0.24	-9.846	-0.0005	-0.70	0.0078	7.85	0.35	-7.91[a]	0.084	-6.82[a]
SH_N*	1955	0	-0.30	-15.40	0.0027	6.84	0.0066	7.56	0.36	-7.79[a]	0.091	-5.91[a]

Note: The regression model for the unit root tests is defined by the following equations: 1) $y_t = \mu + \beta t + \gamma DT_t^* + \tilde{y}_t$, where $DT_t^* = 1(t > T_b)(t - T_b)$ and 2) $\tilde{y}_t = \alpha \tilde{y}_{t-1} + \sum_{i=1}^{k} c_i \Delta \tilde{y}_{t-1} + e_t$. The symbols used are defined as follows: T_b is the estimated time of the break; k is the number of lagged differences added to correct for serial correlation; $S(\hat{e})$ is the standard error of the regression; $\hat{\mu}, \hat{\beta}, \hat{\gamma}$ are the regression coefficients of the trend function and $t_{\hat{\mu}}, t_{\hat{\beta}}, t_{\hat{\gamma}}$ the corresponding t-statistic values. $\hat{\alpha}$ is the sum of the autoregressive coefficients and $t_{\hat{\alpha}}$ is the Perron (1997) unit root test statistic. $t_\alpha(\lambda_{tr}^{AO})$ is the Kim and Perron (2009) unit root test. a,b,c,d denotes statistical significance at the 1 %, 2.5 %, 5 % and 10 %, respectively (critical values from Perron, 1997, for the test $t_{\hat{\alpha}}$, and from Perron and Vogelsang, 1993, Table 1, for the test $t_\alpha(\lambda_{tr}^{AO})$).

Table 4

Break date estimates and 95 % confidence intervals for global and hemispheric temperatures.

	NASA	HadCRUT3
Globe	1978	1971
	(1971,1985)	(1962,1980)
NH	1985	1984
	(1979,1991)	(1977,1991)
SH	1923	1955
	(1914,1932)	(1945,1965)
SH*	1955	-
	(1945,1965)	

On the contrary, using the HadCRUT3 the break date is estimated to occur in 1955, a break date that is statistically different from both the estimate using the NASA dataset and that of Gay-Garcia et al. (2009).

These differences can be explained by analyzing the sum of the squared residuals (SSR) of the regressions used to estimate the beak date. The estimates of the SSR show two minima in both the NASA and HadCRUT3 series. Figure 2 shows the results to be sensitive to the sample period used: when the sample of the HadCRUT3 and NASA series are the same (Figure 2b), the global minimum occurs around 1915 and is very similar to that of NASA (Figure 2a). However, when the full sample of the HadCRUT3 is used (1850-2010) the global and local minima exchange places: the global minimum occurs in 1955 and the local one takes place during the first three decades of the century (Figure 2c). This behavior suggests the existence of a second break in the slope of the trend function and that the longer sample of the HadCRUT3 provides a better estimate of the break date. For this reason, Table 3 also includes the results for the NASA southern hemisphere temperature series when choosing 1955 as the break date (labeled SH_N*). As can be seen from the results, the rejection of the null of a unit root is robust to this change in the break date.

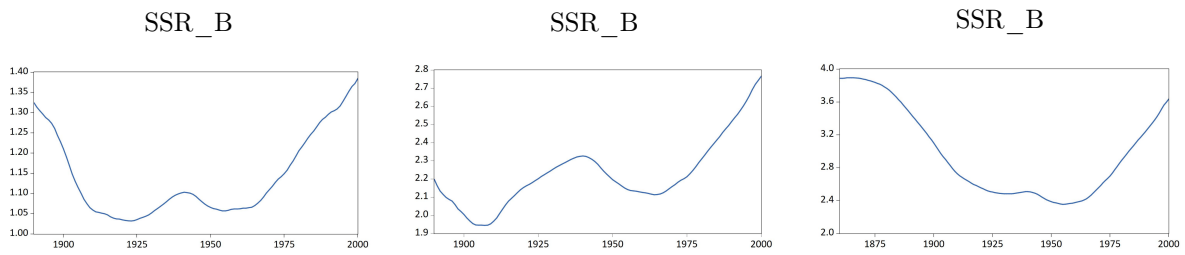

(a) NASA **(b)** CRU (sample 1880-2010) **(c)** CRU (sample 1850-2010)

Figure 2. Sum of the squared residuals of the regressions used to estimate the break date for the Southern Hemisphere temperature series from the NASA and HadCRUT3 datasets with different samples.

The total increase in global and hemispheric temperatures is estimated to be practically the same from the HadCRUT3 and NASA datasets: near 0.8°C, 1°C and 0.7°C, for the global, northern and southern hemisphere temperatures. Also, from both datasets about 60 % of the observed warming in the global and northern hemisphere has occurred in a short period of time, the last three to four decades in the case of the global average and in the last twenty-five years for the northern hemisphere. The rate of increase in the global and northern hemisphere temperatures in the post-break period has been approximately 1.7°C and 2.7°C per century, respectively. In the case of the southern hemisphere, most of the warming has occurred since the last 55 years (between 64 % and 82 %, depending on the dataset) and the rate of increase in temperature has been approximately 1°C per century. The magnitudes of the pre- and post-break slopes reveal important differences between datasets, particularly in the case of the southern hemisphere for the pre-break period. For global and northern hemisphere temperatures, the estimates of the pre-break slope using NASA's dataset are 77 % and 40 % larger than those using the HadCRUT3 dataset, and 145 % larger in the case of the southern hemisphere temperature. The differences in the estimated post-break slopes are small in the cases of global and northern hemisphere temperatures (5 % and 1 %, respectively) but for the NASA dataset the southern hemisphere post-break slope is about 34 % smaller than that of the HadCRUT3's. The large differences in the estimates of the southern hemisphere pre- and post-break slopes using NASA and HadCRUT3 datasets can be due to the inclusion of a wider coverage in the sea-surface temperature dataset in the later (see Brohan et al., 2006).

According to these estimates observed temperatures have experienced a large increase in the rate of growth since the mid-20th century. For the NASA dataset the post-break rate of warming (i.e., the pre plus post-break slopes) is 3.3, 5.6 and 2.4 times larger than the pre-break estimate for global, northern and southern hemisphere, respectively. For the HadCRUT3 dataset these rates are 6.2, 8.1 and 9 times larger than the pre-break slope, in that order. As will be shown in the next sections, these abrupt increases represent the response of the climate system to a doubling in the rate of growth of the observed forcing. These changes concur with the important characteristics of observed warming that have been previously reported (Gay-Garcia et al., 2009): temperature series can be better described as trend stationary processes with a one-time permanent shock that cannot be interpreted as part of the natural variability; climate

change has occurred in two stages, the first consisting in a moderate rate of warming and a second one showing a much larger rate of increase occurring rather abruptly in a short period of time. Estrada et al. (2013a) have shown that these time-series characteristics are also present in the 20th Century Climate Experiment simulations conducted for the IPCC's Fourth Assessment Report (IPCC-WGI, 2007).

2.2. Results for the Observed Radiative Forcing

In this section, the time series properties of radiative forcing series are investigated using the same econometric techniques applied before to temperature series. The results are robust to different definitions of the radiative forcing trend and show that the common assumption of forcing variables being integrated processes is not supported by the data. The radiative forcing series used were published by Hansen et al. (2011) and are available at the NASA Goddard Institute for Space Studies website. The database covers the period 1880-2010 and includes the following variables (in W/m2): well mixed greenhouse gases, WM-GHG (carbon dioxide (CO2), methane (NH4), nitrous oxide (N2O) and chlorofluorocarbons (CFCs)); ozone (O3); stratospheric water vapor (H2O); solar irradiance (SOLAR); land use change (LAND_USE); snow albedo (S_ALBEDO); stratospheric aerosols (STRAT_AER); black carbon (BC); reflective tropospheric aerosols (R_AER); and the indirect effect of aerosols (AIE). As can be seen from Figure 3, with the exception of stratospheric aerosols, all time series show a clearly nonstationary behavior in their level with large changes in their rates of growth.

Because the interest relies on investigating the relationship between temperature and anthropogenic and natural forcing series, different "aggregate forcing trends" that may be driving the observed changes in global and hemispheric temperatures are constructed and analyzed in this section, instead of focusing on the time-series properties of the individual forcing variables. We use this approach mostly because we want to extract the overall influence of total anthropogenic versus natural forcings on temperatures, not the specific effect of various individual components keeping in mind that CO2 stands out as the dominant one. In addition, these radiative forcing trends are used to estimate the multivariate models presented in the next section, as a substitute for the original forcing variables, which permits avoiding severe multicollinearity problems. Two approaches were adopted for constructing different "forcing trends". The first consists in simply adding the forcing variables to construct the forcing trend. This is the standard procedure in climate modeling. Three forcing trends using this approach were considered (Figure 4): 1) well-mixed greenhouse gases (WM_GHG) which represents the dominant human contribution to the observed radiative forcing; 2) GHG_SOLAR, composed of WM_GHG plus SOLAR, represents the main anthropogenic and natural forcing variables; 3) ALL_FORCING includes all of the human and natural forcing that contribute to the forcing trend (GHG_SOLAR plus H2O, LAND_USE, S_ALBEDO, BC, R_AER and AIE). Note that STRAT_AER was not added to construct the forcing trend given that it is stationary around a constant. Instead, this variable is introduced as another independent variable in the regression models presented later. As can be seen from Figure 4, WM_GHG is the most important variable contributing to the increase in radiative forcing. Solar forcing mainly contributes to adding variability to the WM_GHG

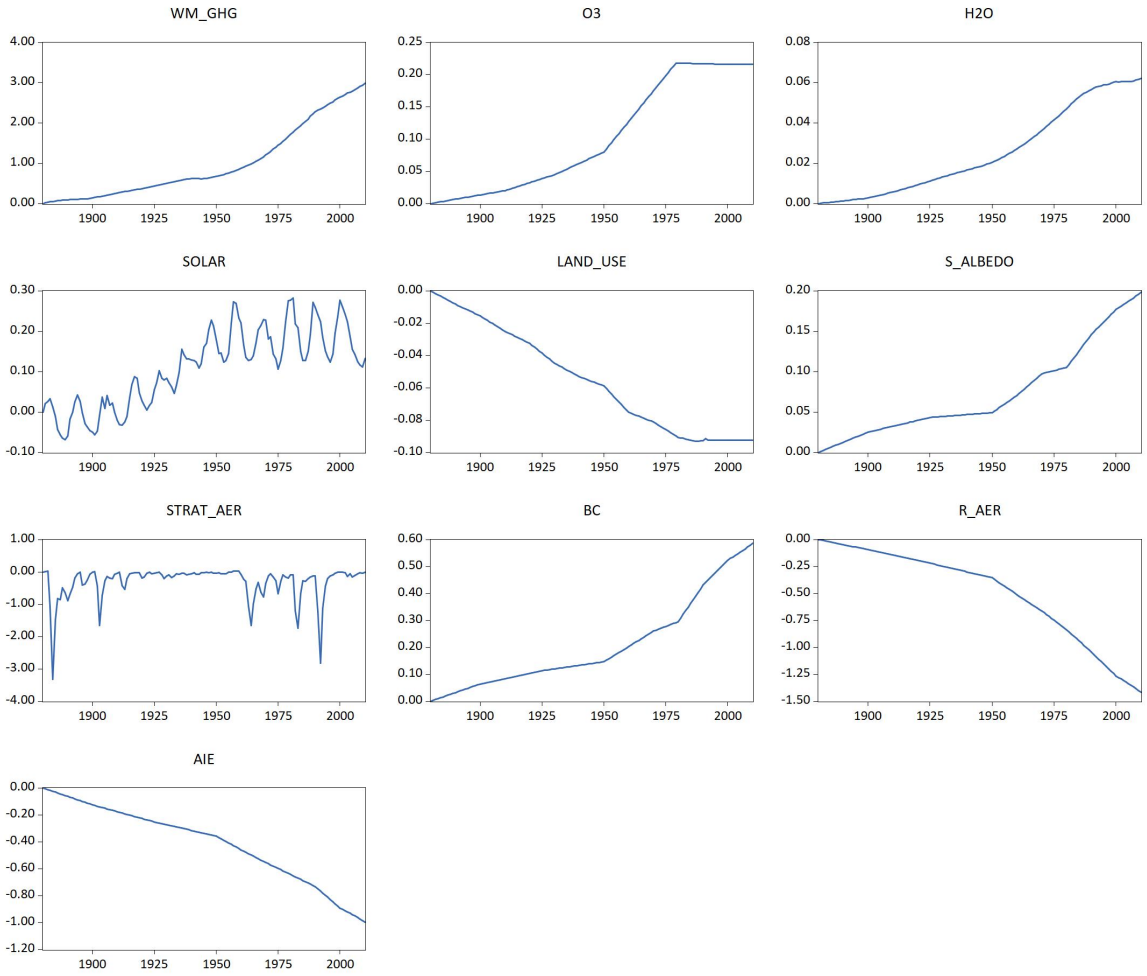

Figure 3. Time series plot of the forcing variables: well mixed greenhouse gases (WM_GHG); ozone (O3); stratospheric H2O (H2O); solar irradiance (SOLAR); land use change (LAND_USE); snow albedo (S_ALBEDO); stratospheric aerosols (STRAT_AER); black carbon (BC); reflective aerosols (R_AER); aerosols indirect effect (AIE). Units are watts per squared meter.

trend, particularly imparting the well-known Schwabe 11 year cycle (IPCC-WGI, 2007). The ALL_FORCING variable shows that the sum of forcing factors other than greenhouse gases and solar have a negative net effect on the forcing trend. The reduction in the rate of growth of the total radiative forcing is particularly important since the 1990's, primarily due to the direct and indirect effects of tropospheric aerosols.

The second approach consists in applying a principal component analysis to reduce the dimensionality and extract the principal modes of variation, in particular the trend mode. The first principal component explains 83.32 % of the variance of the radiative forcing and, as can be seen in Figure 5, it represents the forcing trend. As revealed by the eigenvector associated to this principal component, the forcing trend is a mixture of human and natural factors with similar weights, except for stratospheric aerosols whose weight is close to zero (Table 5). The forcing trend is thus a combination of all forcing series excluding stratospheric aerosols. The

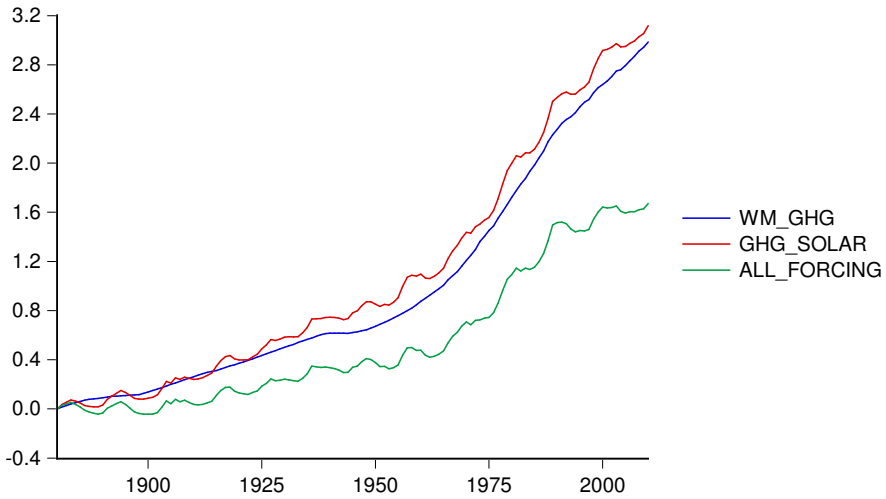

Figure 4. Forcing trends constructed as the sum of the radiative forcing variables; units are watts per squared meter.

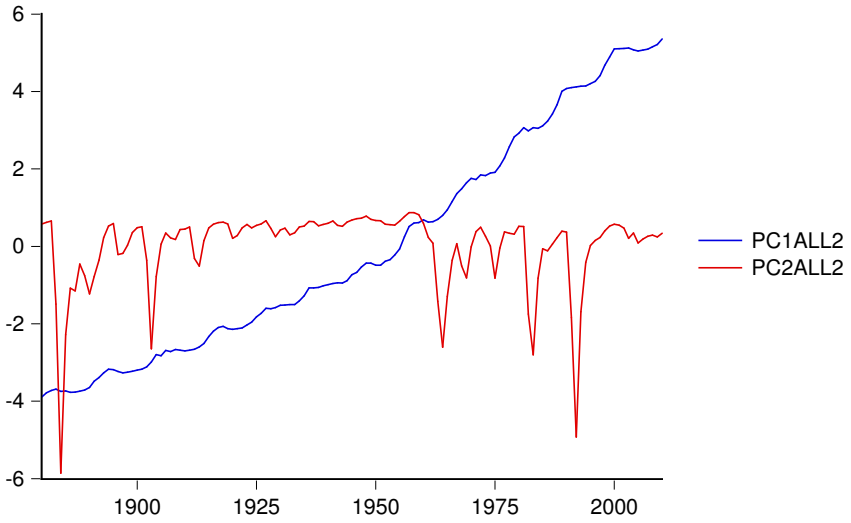

Figure 5. First and second principal components of the set of radiative forcing series.

second principal component (also depicted in Figure 5) explains only 10.15 % of the variance and it mainly represents the stratospheric aerosols forcing (Table 5). The remaining principal components contribute only marginally to explaining the variance of this set of time series and therefore are excluded from subsequent analyses.

The time series properties of the series constructed using both approaches are analyzed in the rest of this section and will be used for the multivariate models presented subsequently. Note that while the first approach has a clear physical meaning and allows for easier attribution of the observed warming to different natural and anthropogenic factors, the second approach provides a clearer separation of the trend mode from the other modes of variability.

Table 5
Eigenvectors of the first two principal components of the set of radiative forcing.

Variable	PC1	PC2
WM_GHG	0.340	-0.036
SOLAR	0.272	0.120
STRAT_AER	0.011	0.988
H2O	0.345	-0.041
BC	0.339	-0.015
R_AER	-0.343	0.027
AIE	-0.345	-0.018
O3	0.339	-0.060
S_ALBEDO	0.340	-0.016
LAND_USE	-0.331	-0.049

As in the previous section, standard ADF unit root tests were applied to the forcing variables. The ADF tests included in all cases a constant and a trend as the deterministic components with the exception of the STRAT_AER and PC2 variables for which only a constant was included. The results in Table 6 show that while PC2 and STRAT_AER can be considered as stationary around a constant, the unit root null hypothesis cannot be rejected at any conventional levels for all the "forcing trend" variables. Again, other most recent unit root tests proposed by Ng and Perron (2001) also suggest the same results. Nevertheless, as mentioned in the previous section, standard unit root tests can be severely affected by the presence of structural breaks in the trend function, particularly when the break occurs in the slope parameter. Figure 4 and 5 strongly suggest that the rate of growth of these variables has not remained constant over the sample period, and thus standard unit root tests may not be adequate for investigating their time-series properties.

The existence of structural breaks in the slopes of the trend function of these forcing trend variables was tested using the Perron and Yabu (2009) procedure and, as shown in Table 7, for all variables the null of parameter stability is strongly rejected. These results clearly suggest that the finding of unit roots in the forcing variables reported in some of the previous publications may due to the effect that breaks in the slope of the trend function have on standard unit root tests. As in the case of global and hemispheric temperatures, allowing for the presence of a one-time structural change in the slope of the trend function changes the conclusions markedly. As shown in Table 8, the Perron (1997) and Kim and Perron (2009) tests applied to the forcing trend variables defined above strongly reject the null of a unit root in favor of trend stationary processes with one permanent break in their rate of growth. This finding has important implications for the multivariate modeling of temperatures and radiative forcing variables. The results indicate that there are no differences in the order of integration of these variables, all of them can better be described as trend stationary processes. Therefore, the existence of long-term relationships can be tested using standard regression models and there is no need to invoke for this purpose cointegration methods that require the assumption of unit root processes in temperature and forcing series.

The point estimate of the break date for all the forcing trend variables constructed under the first approach is 1960. This break occurs after the small decline in WM-GHG around WWII and

Table 6
Standard Augmented Dickey-Fuller test applied to the various forcing trend.

Series	ADF test statistic
WM_GHG	-2.74
GHG_SOLAR	-2.76
ALL_FORCING	-2.73
STRAT_AER	**-4.92**
PC1	-2.31
PC2	**-4.80**

Note: The AIC information criterion was used for determining the lag length, and the deterministic regressors were a constant and a trend, except for PC2 and STRAT_AER for which only a constant was included. Figures in bold denote statistical significance at 5 % level.

Table 7
Perron and Yabu (2009) test for a structural change in the trend function allowing an integrated or stationary noise component.

Series	Exp-Wald statistic value
WM_GHG	62.79[a]
GHG_SOLAR	5.41[a]
ALL_FORCING	5.63[a]
PC1	2.65[a]

Note: a, b, c denote statistical significance at the 1 %, 5 % and 10 %, respectively.

the subsequent recuperation of European economies (Figure 4). For PC1, the break date occurs 13 years earlier, in 1947. The estimated post-break rates of growth of the radiative forcing variables are of much larger magnitude compared with those before the pre-break: for WM_GHG the increase in the rate of growth is 334 %; 213 % for GHG_SOLAR and 345 % for ALL_FORCING. In the case of PC1, the post-break rate of growth is 107 % larger than it was prior to the occurrence of the break. It is interesting to note that according to the 95 % confidence intervals estimated using the Perron and Zhu (2005) procedure (Table 9), the break dates of the forcing variables are not statistically different form the break date found in the southern hemisphere temperature series. Also, when applying the Perron and Yabu (2009) test on the forcing trends to the subsample 1880-1930, another break in the slope can be found at the beginning of the 20th century which is very close to the one that can be found in the southern hemisphere temperature series using the NASA dataset and when restricting the HadCRUT series to 1880-2010 (Table 4 and Figure 2). In the case of global and northern hemisphere temperatures, the break in the slope occurs later in the century and there is no evidence of another break at the beginning of the century. Despite these differences, it is shown in the next section that the long-term movements of all these variables are so closely related that the observed temperature and forcing trends cancel out, producing stationary residuals. Temperature and forcing variables share the same long-term trend. The forcing signal of well-mixed greenhouse gases is present in all temperature

Table 8

Unit root tests applied to the "forcing trend" variables allowing for a one-time break in the trend function.

Series	T_b	k	$\hat{\mu}$	$t_{\hat{\mu}}$	$\hat{\beta}$	$t_{\hat{\beta}}$	$\hat{\gamma}$	$t_{\hat{\gamma}}$	$\hat{\alpha}$	$t_{\hat{\alpha}}$	$S(\hat{e})$	$t_\alpha(\hat{\lambda}_{tr}^{AO})$
WM_GHG	1960	7	-0.0343	-4.08	0.0105	64.95	0.0351	87.76	0.9009	-4.24[b]	0.040	-3.96[b]
GHG_SOLAR	1960	2	-0.1459	-8.20	0.0144	44.50	0.0307	42.37	0.8359	-5.59[a]	0.022	-4.86[a]
ALL_FORCING	1960	2	-0.0852	-5.34	0.0064	20.82	0.0221	28.98	0.8365	-4.58[a]	0.076	-4.24[b]
PC1	1947	2	-4.0457	-110.44	0.0496	61.45	0.0533	35.52	0.6901	-7.37[a]	0.162	-5.85[a]

Note: The regression model for the unit root tests is defined by the following equations: 1) $y_t = \mu + \beta t + \gamma DT_t^\star + \tilde{y}_t$, where $DT_t^\star = 1(t > T_b)(t - T_b)$ and 2) $\tilde{y}_t = \alpha \tilde{y}_{t-1} + \sum_{i=1}^{k} c_i \Delta \tilde{y}_{t-1} + e_t$. The symbols used are defined as follows: T_b is the estimated time of the break; k is the number of lagged differences added to correct for serial correlation; $S(\hat{e})$ is the standard error of the regression; $\hat{\mu}, \hat{\beta}, \hat{\gamma}$ are the regression coefficients of the trend function and $t_{\hat{\mu}}, t_{\hat{\beta}}, t_{\hat{\gamma}}$ the corresponding t-statistic values. $\hat{\alpha}$ is the sum of the autoregressive coefficient and $t_{\hat{\alpha}}$ is the Perron (1997) unit root test statistic. $t_\alpha(\lambda_{tr}^{AO})$ is the Kim and Perron (2009) unit root test. a, b, c, d denotes statistical significance at the 1 %, 2.5 %, 5 % and 10 %, respectively (critical values from Perron, 1997, for the test $t_{\hat{\alpha}}$, and from Perron and Vogelsang, 1993, Table 1, for the test $t_\alpha(\lambda_{tr}^{AO})$).

Table 9

Break date estimates and 95 % confidence intervals for the forcing trend variables.

	Break date	
WM_GHG	1960	(1958,1962)
GHG_SOLAR	1960	(1957,1963)
ALL_FORCING	1960	(1955,1965)
PC1	1947	(1944,1950)

series. It is especially pronounced for southern hemisphere temperatures for which the signal is much clearer given that it is dominantly covered by the ocean, known to modulate temperature variability, making it more stable around the long-term trend (Jones et al., 1986a,b; Hansen et al., 1987).

The difference in the estimates of the break dates in the northern hemisphere, southern hemisphere and global temperatures can be accounted for by the effect of the Atlantic Multidecadal Oscillation (AMO) which represents ocean-atmosphere processes naturally occurring in the North Atlantic with a large influence over the northern hemisphere and global climates. As shown in Estrada et al. (2013b), when this effect is filtered out the break dates for global and northern hemisphere from the HadCRUT3 dataset are estimated to occur in 1955 and 1959, respectively. The NASA dataset leads to similar estimates of the break dates, namely 1956 and 1968. Hence, once the AMO is accounted for, all temperature series have nearly the same break dates, which are very close to those of the forcing variables.

3. Common Breaking Trends

We first use a simple approach to test for common trends in temperatures and forcing variables that consists in estimating an Ordinary Least Squares (OLS) regression and conducting a standard ADF test on the residuals. This is similar to the Engle-Granger (1987) two-steps cointegration test but for trend-stationary variables (so the critical values are those tabulated with no deterministic term included). The basic idea is to detrend global and hemispheric tem-

peratures with the forcing trends and test if any non-stationarity remains in the residuals. With stationary residuals, both temperatures and radiative forcing share the same long-term trend and the observed warming during the 20th century can be attributed to anthropogenic activities. We use the regression:

$$T_{i,j,t} = \alpha + \beta FT_{r,t} + \varepsilon_t \tag{1}$$

where $T_{i,j,t}$ are the observed average temperatures for the global, northern and southern hemisphere ($i = 1, 2, 3$) and for the NASA and HadCRUT3 datasets ($j = 1, 2$), while $FT_{r,t}$ are the forcing trends. The way forcing trends were defined above is useful to separate the importance of human and natural factors in the observed warming trend: WM_GHG is mostly human-made, GHG_SOLAR represent a combination of the main human and natural forcing factors, and ALL_FORCING the sum of all natural and anthropogenic forcing factors. If the residuals from regression (1) obtained using WM_GHG are non-stationary but stationary when using the GHG_SOLAR or ALL_FORCING variables, this would be evidence about the strong contribution to observed warming by non-human-induced forcing factors. On the opposite, if the residuals are stationary when temperatures are detrended using WM_GHG only, the interpretation is then that anthropogenic factors are the dominant cause of global warming. To further highlight the importance of human role in the observed warming of the 20th century, a combination of the forcing trends defined above is also considered: ALL_FORCING minus WM_GHG (hereafter ALL_FORCING*) which represents all forcing with the exclusion of the most important anthropogenic forcing.

Table 10 shows the slope coefficient estimates of regression (1) as well as the associated t-statistic value and the coefficient of determination for each combination of temperature and forcing trends. The first thing that transpires from these results is that the slope coefficients in all the estimated regressions using ALL_FORCING* are nonsensical because they imply a negative relation between radiative forcing and temperature that is not physically possible. The total forcing trend when excluding WM_GHG has a strong negative trend that cannot reproduce the observed warming. Hence, the observed warming cannot be explained in a physically consistent manner if the well-mixed greenhouse gases are excluded. The last column of Table 10 presents the value of the standard ADF test specified with no deterministic terms when applied to the residuals of regression (1). A rejection of the null hypothesis of a unit versus the alternative of stationarity is evidence that the trends in temperatures and forcings are common. If they were not, and given the fact that it has been established that the trends are non-linear, this would induce residuals having a non-constant mean, which would induce a bias in the sum of the autoregressive coefficients towards one and, hence, a non-rejection of the null hypothesis. These results show strong support for the common trend hypothesis between temperatures and radiative forcing, and in particular for the contribution of greenhouse gases to the observed warming. Even when the forcing trend is limited to WM_GHG, the ADF test is considerably larger (in absolute value) than the critical value at the 1 % significance level, providing strong evidence that observed temperatures follow the same long-term path as the human-made forcing, which has been increasing very rapidly since 1960. Strong evidence in favor of a common trend is shown for global and hemispheric temperatures and for both NASA and HadCRUT3 datasets. The

Table 10

Estimated slope coefficient, goodness of fit measure, and ADF test on the residuals of regression (1) for different forcing trends.

		Global Temperature			NH Temperature			SH Temperature		
	Forcing Trends	β	R^2	ADF	β	R^2	ADF	β	R^2	ADF
NASA DATASET	WM_GHG	0.258	0.81	-3.96	0.283	0.70	-4.05	0.232	0.84	-7.45
		(23.59)		(2)	(17.27)		(1)	(26.01)		(0)
	GHG_SOLAR	0.241	0.82	-4.03	0.264	0.70	-4.05	0.217	0.85	-7.98
		(24.07)		(2)	(17.46)		(1)	(26.74)		(0)
	ALL_FORCING	0.409	0.80	-3.76	0.447	0.68	-3.86	0.371	0.84	-7.72
		(22.86)		(2)	(16.67)		(1)	(25.99)		(0)
	PC1	0.079	0.79	-3.52	0.086	0.67	-3.70	0.071	0.83	-7.47
		(22.14)		(1)	(16.24)		(1)	(25.31)		(0)
	All Forcing	-0.664	0.79	-6.07	-0.735	0.69	-4.28	-0.593	0.80	-6.79
	Except GHG	(-22.06)		(0)	(-16.96)		(1)	(-22.85)		(0)
		Global Temperature			NH Temperature			SH Temperature		
	Forcing Trends	β	R^2	ADF	β	R^2	ADF	β	R^2	ADF
HadCRUT3 DATASET	WM_GHG	0.255	0.77	-5.85	0.280	0.71	-5.20	0.231	0.74	-5.97
		(21.05)		(0)	(17.59)		(0)	(19.40)		(1)
	GHG_SOLAR	0.238	0.78	-5.87	0.261	0.71	-5.23	0.215	0.74	-5.95
		(21.14)		(0)	(17.73)		(0)	(19.36)		(1)
	ALL_FORCING	0.409	0.78	-5.82	0.444	0.70	-5.06	0.374	0.76	-6.20
		(21.15)		(0)	(17.18)		(0)	(20.27)		(1)
	PC1	0.077	0.74	-5.28	0.085	0.68	-4.86	0.069	0.70	-4.07
		(18.92)		(0)	(16.39)		(0)	(17.34)		(2)
	All Forcing	-0.650	0.74	-5.50	-0.722	0.69	-5.19	-0.579	0.69	-5.77
	Except GHG	(-18.98)		(0)	(-16.92)		(0)	(-1.75)		(0)

Note: Figures in parentheses show the t-statistic values except for the ADF in which case it shows the number of lags to correct for serial correlation chosen using the BIC criterion. The critical values for the ADF test are: -2.583 (1%), -1.943 (5%), -1.615 (10%).

results when using the variable PC1 is of special interest because a principal component analysis permits extracting the trend mode in a way that it is more clearly separated from other modes of variation in the multivariate forcing dataset. Hence, it may provide a better representation for the secular movement of the forcing during the sample period. Again, the results indicate a strong long-term relationship between temperature and radiative forcing. Hence, the common trend finding is not sensitive to the way the forcing trend is constructed provided WM_GHG is included.

Figure 6 shows the observed global and hemispheric temperatures from the NASA and HadCRUT3 datasets and the corresponding fitted temperatures obtained from regression (1). It shows that the different definitions of the forcing trend describe very well the long-term movement of all temperature series, irrespective of the dataset and forcing trend considered. Note that the fit produced by WM_GHG reproduces the southern hemisphere temperature so closely

that it almost appears to be a running-mean of temperature. The fit is also very good for global and northern hemisphere temperatures, though not as good as for the southern hemisphere. The northern hemisphere's temperature shows larger variability around its long-term trend because of large ocean-atmosphere cycles that are part of the natural variability over the North Atlantic (notably the AMO) and also the differences in the percentage of land-continent (Schlesinger and Ramankutty, 1994; Kerr, 2000; Knudsen et al., 2010).

Figure 6 also shows the ALL_FORCING plus START_AER and the PC1 plus the PC2 fits (for the global temperature series of the HadCRUT3 dataset, PC2 was not significant and not included). The variables associated with volcanic eruptions have an important effect on temperature variability over the northern hemisphere and global temperatures. Stratospheric aerosols were not significant for the southern hemisphere. Figure 6 illustrates other important common characteristics of temperatures and forcing trends, being more evident for the southern hemisphere. For example, the reported cooling or slowdown of warming shown by all temperature series during 1940-1975 (e.g., Jones et al., 1986a,b,c; Hansen et al., 1987; Tol and De Vos, 1998) also coincides with a slowdown in the well-mixed GHG forcing during the same period. The slowdown in the warming during the last two decades also matches with the deceleration in the increase of the well-mixed greenhouse gases forcing mainly in CFCs due to international regulation (more clearly seen in the southern hemisphere temperature), see Estrada et al. (2013b). Finally, as discussed above, the structural break found in the NASA's southern hemisphere temperature (and in the HadCRUT3 data when the sample is restricted) is also present in WM_GHG.

The evidence presented in this section indicates that the WM_GHG forcing had a determinant role in the observed warming during the last century and dictates the long-term movement in observed temperatures. The changes in aerosols, albedo and other forcing factors contributed somewhat to reducing the warming particularly since the second part of the 20th century. The solar cycles and the volcanic forcing are the main contributors to the variability around the well-mixed greenhouse forcing trend. Figure 7 illustrates these facts by showing the individual contribution of well-mixed greenhouse gases, solar and solar plus other forcing factors to the observed northern temperature series (NASA). The contributions of these variables to the observed warming were obtained by taking the differences between the fitted temperatures shown in Figure 6. The results are similar for global and southern hemisphere temperatures and therefore are not shown. While the WM_GHG have produced an increase of 0.85°C in the northern hemisphere temperature over the period 1880-2010, the solar forcing produced an increase in temperatures around 0.06°C from 1880 to 1960 and then a cooling of more or less the same magnitude from 1961 to 2010. The joint contribution of all forcing except WM_GHG amounts to a decrease of around 0.1°C from 1880 to 2010. That is, the net contribution of all forcing factors other than WM_GHG has been a slight cooling of around 10 % of the warming caused by the WM_GHG increase.

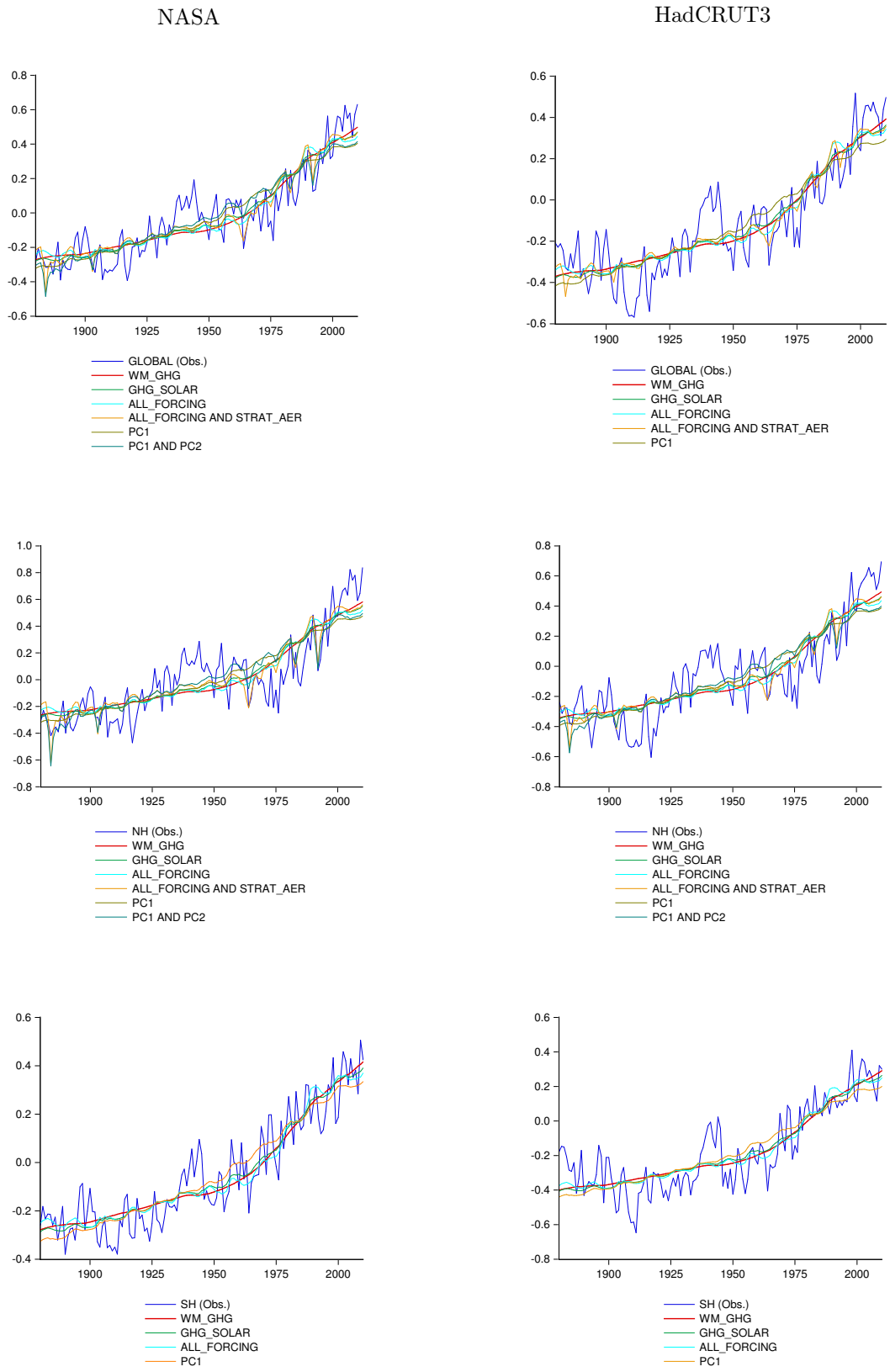

Figure 6. Observed and fitted temperatures using different definitions of the forcing trend.

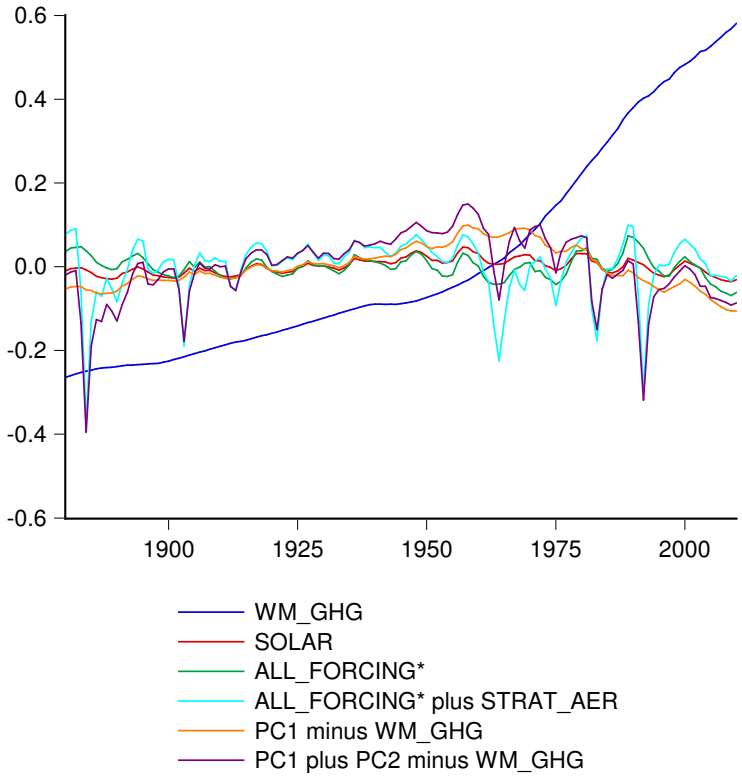

Figure 7. Contributions of different combinations of the forcing trend to the observed warming in the northern hemisphere temperature.

In light of the strong evidence for a long-term relation between forcing and temperature variables, the results indicate that the break in the forcing trend caused the subsequent breaks in temperature series. Table 11 presents a comparison of the post- and pre-break values of the slope of the trend for the forcing and temperature series. In all cases the breaks in temperature series are more than proportional to the break in the forcing variable, irrespective of the forcing trend and of the temperature dataset. For example, for the case of PC1, a doubling in the rate of growth of the forcing produced a post-break slope in the global mean temperature between 4.3 (NASA) and 7.2 (HadCRUT3) times its previous value. For the northern hemisphere the response to the break in the forcing trend is even larger ranging from 6.6 (NASA) and 9.1 (HadCUT3) times its pre-break slope, while for the southern hemisphere the post-break slope is between 3.4 and 10 times its first slope value. Due to natural variability processes and climate dynamics, the breaks in the slope of the forcing manifested themselves with different time lags in global and hemispheric temperatures. The break had an impact on the southern hemisphere almost simultaneously, while for the northern hemisphere and global series these breaks occurred about 35 and 24 years later, respectively.

Table 11
Comparisons of the post- and pre-break values of the slope of the trend for the forcing and temperature series for the HadCRUT3 (C) and NASA (N) datasets.

Forcing trend	Post-break slope compared to its pre-break value
WM_GHG	334 %
GHG_SOLAR	213 %
ALL_FORCING	345 %
PC1	107 %
Temperature	**Post-break slope compared to its pre-break value**
G_C	718 %
NH_C	910 %
SH_C	1000 %
G_N	431 %
NH_N	660 %
SH_N	344 %

4. Short-Run Dynamics and Granger-Causality Tests

To test for the existence of feedback processes in the short-run dynamics of forcing and temperature variables, a vector autoregressive model (VAR) was estimated using the detrended data of the PC1 forcing and of the NASA's global and hemispheric temperatures, as well as the Southern Oscillation Index (SOI) as endogenous variables and PC2 and a constant term as exogenous. The best VAR models estimated for both hemisphere and global temperature series are of order 3 and misspecification testing shows that they are statistically adequate (no autocorrelation, no heteroskedasticity, and residuals approximately normal). These models also satisfy the stability condition as the inverse roots of the characteristic polynomials lie inside the unit circle in all cases. Table 12 presents the results of Granger Causality tests. They show that the detrended forcing (PC1) does not Granger-cause detrended global or hemispheric temperatures, and that the detrended global or hemispheric temperatures also do not Granger-cause detrended PC1. Hence, the forcing trend, here represented by PC1, has a strong role defining the long-term evolution of global and hemispheric temperatures but does not contribute to the short-term dynamics and no significant short-term feedback processes is present, at least with the annual frequency considered. The results are the same using any of the forcing trends considered (as long as WM-GHG is included). Hence, the forcing trends are exogenous. For an alternative perspective on causality from radiative forcing and temperatures, see Estrada and Perron (2019).

5. Time Series Models for Global and Hemispheric Temperatures Series

In this section, statistically adequate models for global and hemispheric temperatures for the NASA and HadCRUT3 datasets are presented. It is shown that parsimonious time-series models can provide a very good fit for observed global and hemispheric temperature series and produce basic estimates of climate sensitivity within ranges reported in the literature using different methods. The models attempt to capture both the short and long-term dynamics: the secular

Table 12
Results of the Granger Causality tests applied to the detrended northern hemisphere, southern hemisphere and global temperatures, and detrended PC1; NASA dataset.

Dependent variable	Excluded	Test	P-value
NH*	SH*	1.02	0.80
	PC1*	4.34	0.23
	SOI	18.51	0.0003
SH*	NH*	0.88	0.83
	PC1*	2.83	0.42
	SOI	18.84	0.0003
PC1*	NH*	1.02	0.80
	SH*	0.89	0.83
	SOI	4.26	0.24
G*	PC1*	3.90	0.27
	SOI	25.97	0.0000
PC1*	G*	0.08	0.995
	SOI	4.39	0.22

Note: SH and NH represent the southern and northern hemisphere temperatures, respectively. * denotes that the variable has been detrended. G represents global temperatures.

movement in global and hemispheric temperature is captured by the forcing trends that were shown to share their long-term trend with temperature variables, while the short-run dynamics are accounted for by the internal dynamics of temperature series and by some climate indices that are known to have an important role in capturing the inter-annual variability of global and hemispheric temperatures. The general form of the models is represented by the following regression:

$$T_t = \alpha + \beta_1 FT_t + \beta_2 AER_t + \sum_{j=1}^{J} \phi_j T_{t-j} + \sum_{k=0}^{K} \gamma_{k+1} SOI_{t-k} + \sum_{l=0}^{L} \delta_{l+1} NAO_{t-l} + \sum_{m=0}^{M} \eta_{m+1} AMO_{t-m} + \varepsilon_t \quad (2)$$

where T_t is global, northern or southern hemisphere temperature from the NASA and HadCRUT3 datasets. Two sets of models were estimated using different forcing trends and stratospheric forcing. The first set uses the PC1 as the forcing trend (FT) and PC2 as a proxy for the stratospheric aerosols forcing (AER). The second set of models uses ALL_FORCING and STRAT_AER as the forcing trend and the stratospheric aerosols forcing, respectively. For modeling the short- and medium-term dynamics, the general model includes the El Niño/Southern Oscillation (ENSO, denoted here by the SOI), the North Atlantic Oscillation (NAO) and the Atlantic Multidecadal Oscillation (AMO), which are commonly considered as important natural sources of inter-annual global and hemispheric climate variability (Enfield et al., 2001; Hurrell, 1995; Wolter and Timlin, 1998). The number of lags was chosen based on the statistical significance of the parameters and also to have nearly-normal residuals with no autocorrelation or heteroskedasticity and a functional form deemed well specified with stable parameters.

Table 13 shows the estimated coefficients of the proposed models for global and hemispheric temperatures. Although the results of misspecification testing are not shown here, all models

are statistically adequate in the sense that the residuals do not show autocorrelation, they are homoskedastic, normal and the estimated parameters are stable. Note that all coefficients have signs expected from climate physics: the forcing trend has a warming effect, while stratospheric aerosols produce a decrease in temperatures; a negative variation in SOI (for example, the occurrence of an El Niño) produces an increase in temperatures and the contemporaneous values of NAO of AMO are positively related to temperatures. The coefficient of determination R^2 in all of the models is very large, indicating that the models fit the observed data quite well.

The different models show strong similarities indicating robustness of the results; e.g., the data set used (NASA or HadCRUT3) or the definitions of the forcing variables included (PC1 or ALL_FORCING; PC2 or STRAT_AER). Global temperature models typically include significant variables such as the forcing trend, stratospheric aerosols, a lagged value of global temperature, and the contemporaneous values of SOI and AMO. As expected from the results in the previous sections, the short-term dynamics are more complex in the northern hemisphere temperatures for which the models, in general, include the same variables as for the global temperature models plus a second order lagged value of AMO and a contemporaneous value of NAO. On the other hand, the models for the southern hemisphere temperatures show simpler short-term dynamics for which only the contemporaneous value of SOI and AMO and a lagged value of the southern hemisphere temperature are relevant. As discussed previously, the variability of the southern hemisphere temperatures is strongly modulated by the oceans and, hence, less affected by shorter-term processes compared to the global and northern hemisphere temperatures. As in the case of the VAR model in Section 4, for all models of temperature series lagged terms of the forcing trend are not significant, supporting the hypothesis that this variable does not have a significant effect on short-term dynamics. Some differences in the results between the datasets are clearer for the southern hemisphere series, where for the HadCRUT3 series the forcing from stratospheric aerosols is not significant and the AMO is shown to be relevant to explain part of the variability of temperature. These are due to the wider ocean sea-surface temperature coverage of the HadCRUT3 dataset (Brohan et al., 2006).

The estimated long-run effect of the total forcing (excluding the stratospheric aerosols) is very similar regardless of the dataset used: the global temperature estimate differs only by 1.08 % from one dataset to the other, while for the northern hemisphere the difference is 5.86 % and the largest difference (8.11 %) occurs in the estimate for the southern hemisphere, where the two datasets are less similar. The estimates show even smaller differences amounting to less that 3.5 % (0.15 % for global, 3.12 % and 3.44 % for northern and southern hemispheres, respectively). Again, the results are robust to the different datasets and the definition of the forcing variables.

The estimates in Table 13 can provide basic approximations of the climate sensitivity (CS) to changes in the forcing variables. Using the NASA dataset, a volcanic eruption of similar magnitude to that of Mount Pinatubo in 1991 would produce a cooling effect of 0.16°C in global temperatures, and of 0.29°C in the northern hemisphere (the estimates using HadCRUT3 are similar: a cooling of 0.1 and 0.18 for global and northern hemisphere temperatures, respectively). These values are close to those estimated from observations and climate models (Hansen et al., 1996). Basic estimates of CS to a doubling of the atmospheric concentrations of CO2 can also

Table 13
Estimated coefficients and coefficient of determination of regression (2), HadCRUT3 (C) and NASA (N) datasets.

		α	β_1	β_2	ϕ_1	ϕ_2	γ_1	δ_1	η_1	η_2	R^2	$S(\hat{e})$
PC1 and PC2 used	G_N	-0.009	0.054	0.019	0.275	-	-0.030	-	0.346	-	0.930	0.0690
		(-1.43)	(10.17)	(2.95)	(4.19)		(5.17)		(8.08)			
	NH_N	0.008	0.038	0.038	0.358	0.196	-0.020	0.060	0.642	-0.325	0.915	0.0889
		(0.98)	(5.64)	(4.59)	(4.69)	(3.16)	(-2.53)	(3.20)	(9.07)	(-3.93)		
	SH_N	-0.030	0.040	0.013	0.445	-	-0.035	-	-	-	0.886	0.0778
		(-3.77)	(6.90)	(1.91)	(6.02)		(-5.45)					
	G_C	-0.054	0.035	-	0.525		-0.029	-	0.437	-0.225	0.921	0.0744
		(-5.28)	(6.51)		(7.69)		(-4.55)		(8.37)	(-3.66)		
	NH_C	-0.026	0.038	0.021	0.373		-0.029	-	0.575	-0.253	0.917	0.0885
		(2.70)	(5.11)	(2.51)	(4.41)		(-3.78)		(8.64)	(-3.03)		
	SH_C	-0.081	0.031	-	0.535		-0.041	-	0.152	-	0.863	0.0903
		(-6.06)	(6.31)		(8.66)		(-5.64)		(3.36)			
ALL_FORCING and STRAT_AER used	G_N	-0.147	0.283	0.053	0.262	-	-0.028	-	0.327	-	0.933	0.0678
		(-8.59)	(10.47)	(4.30)	(4.06)		(-4.88)		(7.98)			
	NH_N	-0.101	0.264	0.096	0.203	0.158	-0.029	0.040	0.479	-	0.910	0.0915
		(-5.49)	(8.60)	(5.64)	(2.85)	(2.56)	(-3.70)	(2.13)	(7.99)			
	SH_N	-0.134	0.210	0.033	0.426	-	-0.033	-	-	-	0.887	0.0775
		(-6.13)	(6.92)	(2.53)	(5.64)		(-5.14)					
	G_C	-0.169	0.212	0.033	0.448	-	-0.031	-	0.407	-0.186	0.930	0.0705
		(-6.60)	(7.16)	(2.53)	(6.11)		(-5.02)		(7.98)	(-3.12)		
	NH_C	-0.123	0.203	0.059	0.370	0.154	-0.026	0.041	0.602	-0.282	0.912	0.0857
		(-4.41)	(5.37)	(3.66)	(4.48)	(2.44)	(-3.28)	(2.27)	(8.76)	(-3.26)		
	SH_C	-0.204	0.197	-	0.443	-	-0.039	-	0.159	-	0.872	0.0872
		(-7.64)	(7.18)		(6.63)		(-5.56)		(3.62)			

be obtained, although they must be interpreted with care since to estimate CS two equilibrium states should be compared, and the observed climate is not at an equilibrium state (IPCC-WGI, 2007). Rather, observed temperature records describe a climate transient, i.e., a measure of the strength and of the contemporary climate response to greenhouse gas forcing. Hence, the estimated CS are expected to underestimate the "true" value of this parameter and to lie close to the lower end of the CS range produced by climate models and reported in, e.g., the IPCC's Fourth Assessment Report (IPCC-WGI, 2007).

To construct the CS estimates, it is assumed that for a doubling of CO2 atmospheric concentrations the corresponding radiative forcing is ΔQ_{2x} = 4.39 W/m2 (Houghton et al., 1990; Wigley and Raper, 1990). The CS parameter is then estimated by $S = \beta_1/(1-\phi_1-\phi_2)\Delta Q_{2x}$. In order to account for the uncertainty in the estimated parameters β_1, ϕ_1 and ϕ_2, the confidence intervals for S were obtained from Monte Carlo simulations using 10,000 replications based on the parameters and standard errors are shown in Table 13. Table 14 presents the estimated CS for global and hemispheric temperatures for both the HadCRUT3 and NASA datasets. Note that the CS values are very similar for global and hemispheric temperatures irrespective of the dataset

used. As expected, although the estimated mean CS values for global temperature (around 1.7°C with a 95 % confidence interval of 1.21°C to 2.32°C) are consistent with the range of CS estimates using climate models simulations (IPCC-WGI, 2007), they lie on the low end of such range. The estimates are closer to those produced using observations and statistical models (e.g., Kaufmann et al., 2006a; Stern and Kaufmann, 1997b; Tol and De Vos, 1998). The largest response to a doubling of CO2 atmospheric concentrations occurs in the northern hemisphere where the estimated 95 % confidence interval extends from 1.17°C to 3.14°C, with a mean estimate near 2°C. The lowest values for CS are those for the southern hemisphere, ranging from 1.12°C to 2.22°C. But these differences are not statistically significant.

The estimates presented in Table 14 do not take into account a large part of the feedback processes that exist in the climate system and that are incorporated in complex climate models. Therefore, they could seriously underestimate the CS and the hemispheric differences could be larger due to the diverse regional climate feedback processes. To illustrate the importance that these feedbacks can have over CS estimates, consider the following equation to express the climate sensitivity, $S = \Delta T_0/(1-f)$ where f is the feedback factor, which amplify (if $0 < f < 1$) or damp the initial blackbody response of $\Delta T_0 = 1.2°C$ for a CO2 doubling (Knutti and Hegerl, 2008). The typical value for current General Circulation Models has a mean of 0.65 (Knutti and Hegerl, 2008). Using this value for f, climate sensitivity for global temperature would be 4.9°C instead of 1.7°C. The underestimates of the CS presented in Table 14 when compared to the CS range produced by climate models are probably due to several feedback processes that a climate model considers but that statistical models exclude. In addition, as argued above, observed temperature records do not provide information about equilibrium states but merely about a climate transient. It is likely that a large part of the warming induced by changes in radiative forcing during the 20th century has not yet manifested itself in observed temperatures (IPCC-WGI, 2007).

6. Comparison with the Cointegration Model of Kaufmann et al. (2006a)

Kaufmann et al. (2006a) proposed an alternative model for global temperatures. They assumed temperature and forcing series to be integrated processes without breaks and accordingly considered an error-correction model based on a cointegrating relation, labelled CECM. We updated their results using the specification presented in their Table III. The radiative forcing trend is RFAGG: well-mixed greenhouse gases, the direct and indirect radiative forcing of anthropogenic sulfur emissions and solar irradiance. The cointegrating relation between temperatures and RFAGG is

$$T_t = \alpha_1 + \beta_1 RFAGG_t + \mu_t \tag{3}$$

so that μ_t is stationary. Efficient estimates of the parameters are obtained using Dynamic Ordinary Least Squares (DOLS) with one lag and lead terms (Saikkonen, 1991; Stock and Watson, 1993). The results are presented in Table 15. In all cases, the long-run relationship between temperatures and radiative forcing, β_1, is highly significant with magnitude similar across temperature series. The estimates $\hat{\alpha}_1$ and $\hat{\beta}_1$ can then be used to estimate the following error-correction model

Table 14
Climate sensitivity estimates for a doubling of CO2 atmospheric concentrations; HadCRUT3 (C) and NASA (N) datasets.

Dataset	5 %	Mean	95 %
G_C	1.21	1.72	2.32
G_N	1.35	1.69	2.08
NH_C	1.17	1.98	3.14
NH_N	1.32	1.85	2.52
SH_C	1.12	1.58	2.10
SH_N	1.16	1.63	2.22

Table 15
Estimates of the cointegration relation between temperature series and RFAGG using the DOLS estimates with one lag and lead terms.

	α	β
G_N	-0.2679	0.4350
NH_N	-0.2553	0.4799
SH_N	-0.2804	0.3900
G_C	-0.3704	0.4373
NH_C	-0.3357	0.4763
SH_C	-0.4050	0.3985

Note: All entries are significant at the 5 % level. The standard errors were estimated using the Newey-West heteroskedasticity-robust procedure.

by OLS:

$$\begin{aligned}\Delta T_t &= \alpha_2 + \rho\left(T_{t-1} - \left(\hat{\alpha}_1 + \hat{\beta}_1 RFAGG_{t-1}\right)\right) + \textstyle\sum_{i=1}^{k} \delta_i \Delta T_{t-i} + \sum_{i=1}^{j} \phi_i \Delta RFAGG_{t-i} \\ &\quad + \textstyle\sum_{i=1}^{l} \gamma_i SOI_{t-1} + \sum_{i=1}^{m} \psi_i NAO_{t-1} + \mu_1 STRAT\_AER_t + \varepsilon_t\end{aligned} \tag{4}$$

The number of lags were specified as in Kaufmann et al. (2006a, Table III, column(4)), i.e., $k = 2$, $j = 2$, $l = 1$ and $m = 2$. Note that the CECM in Kaufmann et al. (2006a) was tailored for global rather than hemispheric temperatures. However, the results shown below reveal that this specification yields similar results and goodness of fit for Northern Hemisphere (NH) and Southern Hemisphere (SH). Hence, we shall adopt the same model for all temperature series. The parameter estimates of the Error Correction Model (ECM) (4) estimated by OLS are presented in Table 16. They show that many estimates are not statistically significant. Note that with the exception of the contemporary value of SOI all other series included to account for natural variability are not statistically significant, in particular NAO is not significant in the regression for the NH temperatures and it has a negative sign in the regression for global temperatures. The later results are somewhat at odds with what could be expected from climate theory (Hurrell, 1996). These updated results are similar to those presented in Kaufmann et al. (2006a). This could be interpreted as a sign of poor model specification. Nevertheless, since our goal is to

compare our trend-stationary model, labelled TSM, with the CECM proposed by Kaufmann et al. (2006a), we shall keep the same model specification. Finally, it is interesting to note that the coefficients on the lagged values of $\Delta RFAGG_t$ are not statistically significant in neither Table 16 nor in Kaufmann et al. (2006a, Table III). This gives additional support to our results in Section 4 that the radiative forcing trend does not contribute to the short-term dynamics of temperature and that there are no significant short-term feedback processes, at least when considering an annual frequency.

To compare the two models, we consider both their relative in-sample and out-of-sample forecast performance. The trend stationary models (TSM) considered is the one in Table 13 using $ALL\_FORCING$ and $STRAT\_AER$. We report the root mean squared error (RMSE), the Theil Inequality Coefficient (TU), and to assess whether one model has significantly better predictive power, we use the Diebold and Mariano (1995) test (DM) and the S_{2a} test (Lehman, 1975). With $\hat{y}_t$ the forecast of the temperature y_t, the RMSE is $\sum_{t=t_f}^{t_f+h} (\hat{y}_t - y_t)^2 / h$, where t_f is the starting date of the forecasting period and h is the forecast horizon. The TU statistic is $TU = [(\sum_{t=t_f}^{t_f+h} (\hat{y}_t - y_t)^2 / h)/(\sum_{t=t_f}^{t_f+h} \hat{y}_t^2/h)(\sum_{t=t_f}^{t_f+h} y_t^2/h)]^{1/2}$ and has the advantage of being scale invariant and defined between 0 and 1, with zero indicating a perfect forecast. The S_{2a} statistic is defined by $S_{2a} = \sum_{t=1}^{N} I_+ (d_t) - 0.5N/\sqrt{0.25N}$, where $d_t = [y_t - \hat{y}_{t_{TSM}}]^2 - [y_t - \hat{y}_{t_{CECM}}]^2$, with $I_+ (d_t) = 1$ if $d_t > 0$, 0 otherwise, N is the number of forecasts and $\hat{y}_{t_{TSM}}$ denotes the forecast from the TSM model while $\hat{y}_{t_{CECM}}$ is the forecast from the CECM model. The DM statistic is the t-statistic of the OLS estimate of α in the following regression: $d_t = \alpha + e_t$. Significantly negative values of the statistics S_{2a} and DM provide evidence that the the TSM forecasts are statistically more accurate than those of the CECM.

Tables 17-18 present comparisons of the TSM and CECM forecast performances using in-sample one-step ahead (static) and dynamic forecasts from the beginning of the sample to the end. The results are similar and show that the TSM forecasts for G and NH are more accurate (5 % statistical level) than those of the CECM for both the HadCRUT3 and NASA datasets. For SH temperature, the forecast performances of the TSM and the CECM are similar with the exception of the dynamic forecast using NASA in which case the CECM performs better. Table 19 presents the results for an out-of-sample dynamic forecast evaluation. The sample used for model estimation was 1880-1990 and 1991 to 2010 was used as the forecasting period with an horizon of 20 years. The actual values of the explanatory variables were used to generate the forecasts. The results confirm that the forecasts for G and NH from the TSM are significantly more accurate that those from the CECM at the 5 % level; for SH the differences are not statistically significant. In summary, the TSM model provides a better in-sample fit of temperatures and more accurate forecasts for all series with the exception of SH, in which case the forecast performances are not statistically different. The results are robust to the temperature dataset used and the type of forecasts conducted. These findings are consistent with the fact that the TSM model provides a better in sample fit for G and NH temperatures and a nearly equal fit for SH (cf. Tables 13 and 16).

Table 16

Estimates of the error correction model using the specification of Kaufmann et al. (2006a).

	α_2	ρ	δ_1	δ_2	φ_1	φ_2	γ_0	γ_1	ψ_0	ψ_1	ψ_2	μ_1	$S(\hat{e})$
G_N	0.025[b]	-0.42[b]	-0.22[b]	-0.12[c]	-0.27	0.08	-0.036[b]	-0.014	-0.014	0.001	-0.016	0.075[b]	0.081
NH_N	0.036[b]	-0.34[b]	-0.28[b]	-0.07	-0.024	-0.06	-0.039[b]	-0.023[b]	0.006	0.023	-0.021	0.124[b]	0.111
SH_N	0.013	-0.50[b]	-0.15[c]	-0.13	-0.23	0.24	-0.033[b]	-0.008	-0.031[b]	-0.021	-0.012	0.026	0.077
G_C	0.017[c]	-0.34[b]	-0.15	-0.16[b]	-0.23	0.12	-0.046[b]	0.002	-0.023	0.005	-0.023	0.055[b]	0.085
NH_C	0.029[b]	-0.29[b]	-0.18[c]	-0.10	-0.10	-0.26	-0.047[b]	-0.005	-0.006	0.019	-0.027	0.086[b]	0.109
SH_C	0.006	-0.38[b]	-0.15	-0.24[b]	-0.32	0.52*	-0.045[b]	-0.003	-0.037[b]	-0.005	-0.022	0.026	0.087

Table 17

In-sample static (1-step) forecast comparisons of TSM and CECM.

	$RMSE_{TSM}$	$RMSE_{CECM}$	TU_{TSM}	TU_{CECM}	S_{2a}	DM
G_N	**0.0662**	0.0766	**0.1319**	0.1551	-1.5085[c]	-2.5506[b]
NH_N	**0.0886**	0.1052	**1.1538**	0.1836	-2.3959[b]	-3.1437[b]
SH_N	0.0760	**0.0732**	0.1694	**0.1612**	0.6212	1.5453
G_C	**0.0686**	0.0817	**0.1224**	0.1465	-3.2832[b]	-3.3305[b]
NH_C	**0.0826**	0.1040	**0.1411**	0.1791	-2.3958[b]	-3.9456[b]
SH_C	0.0856	**0.0825**	0.1489	**0.1407**	0.0887	0.8271

Note: b, c denote statistical significance at 5 % and 10 % levels, respectively. Bold entries denote the smallest forecast error statistic.

Table 18

In-sample dynamic forecast comparisons of TSM and CECM.

	$RMSE_{TSM}$	$RMSE_{CECM}$	TU_{TSM}	TU_{CECM}	S_{2a}	DM
G_N	**0.0689**	0.0827	**0.1373**	0.1649	-1.6850^{c}	-2.6273^{b}
NH_N	0.0917	0.1212	**0.1592**	0.2098	-2.0492^{b}	-3.7630^{b}
SH_N	0.0834	**0.0781**	0.1860	**0.1695**	1.6860^{c}	2.1102^{b}
G_C	**0.0784**	0.0985	**0.1406**	0.1751	-2.2184^{b}	-3.7735^{b}
NH_C	**0.0927**	0.1345	**0.1589**	0.2323	-3.2832^{b}	-4.8641^{b}
SH_C	0.1007	**0.0953**	0.1760	**0.1610**	1.6860^{c}	0.8895

Note: b, c denote statistical significance at 5 % and 10 % levels, respectively. Bold entries denote the smallest forecast error statistic.

Table 19

Out-of-sample dynamic (20-steps) forecast comparisons of TSM and CECM.

	$RMSE_{TSM}$	$RMSE_{CECM}$	TU_{TSM}	TU_{CECM}	S_{2a}	DM
G_N	**0.0765**	0.1144	**0.0846**	0.1292	-2.5236^{c}	-2.1039^{b}
NH_N	**0.0984**	0.1525	**0.0931**	0.1427	-2.0647^{b}	-2.1600^{b}
SH_N	0.1226	**0.1179**	0.1730	**0.1660**	0.2294	1.1881
G_C	**0.0709**	0.1057	**0.0999**	0.1510	-1.1471	-2.3514^{b}
NH_C	**0.0815**	0.1381	**0.0897**	0.1543	-1.6059^{c}	-3.1927^{b}
SH_C	0.1070	**0.1045**	0.2039	**0.2031**	0.2294	0.5913

Note: b, c denote statistical significance at 5 % and 10 % levels, respectively. Bold entries denote the smallest forecast error statistic.

7. Conclusions

This paper demonstrates the existence of a robust long-run relationship between radiative forcing and global and temperature series, and that the anthropogenic emissions of greenhouse gases have contributed dominantly to the observed warming during the recorded period. The attribution of climate change to anthropogenic activities presented is robust in that it takes into account the most important natural and anthropogenic forcing variables and natural variability modes referred to in the literature, and it is based on the two most important temperature records available.

The univariate time series analysis shows that both temperature and forcing variables are better represented as trend stationary variables with a break in the slope of their trend function in the 20th century that can hardly be interpreted as a part of natural variability. Also, it is shown with multivariate models that these piecewise linear long-term trends cannot be reproduced in a physically acceptable way unless well-mixed GHG are included. The temperature series show a delayed but more than proportional response to the change in the slope of the forcing trend. The large delay in the northern hemisphere is due to the low frequency natural variability produced by ocean/atmosphere processes over the North Atlantic (Estrada et al., 2013b). The tests for a common trend show that temperatures and forcing variables share the same long-term trend, highly influenced by the well-mixed GHG forcing. The observed warming has clearly been

produced by greenhouse gases: about 0.85°C of the observed warming can be attributed to the well-mixed GHG forcing, while solar forcing had a warming effect near 0.06°C until the first half of the 20th century and then a cooling effect of a similar magnitude. The joint contribution of all forcing variables except well-mixed GHG produced a net cooling effect of 0.1°C from 1880 to 2010.

Parsimonious models for the global and hemispheric temperatures able to capture both the short and long-term dynamics are presented and shown to provide a better fit and more accurate forecasts than the error correction model of Kaufmann et al. (2006a). While stratospheric aerosols had a large but short-term cooling effect in the northern hemisphere, the effect of volcanic eruptions is shown not to have been significant in the southern hemisphere. Short-run dynamics are also shown to be different in the northern and southern hemispheres. The former has a more complex short-run dynamics with stronger persistence and a large influence of ENSO, NAO and AMO. The southern hemisphere temperature has a simpler dynamic in which the excursions from its secular trend are smaller and are mainly influenced by ENSO. The climate sensitivity estimates for a doubling in the CO2 atmospheric concentrations are within the 1.5°C-4.5°C range commonly accepted. This paper provides strong evidence on the direct attribution of climate change to anthropogenic activities using observed temperatures, forcing variables and statistical methods.

References

Brohan P., Kennedy J., Harris I., Tett S., and Jones P. (2006). Uncertainty estimates in regional and global temperature changes: a new dataset from 1850. *Journal of Geophysical Research 111*, D12106.

Dickey D., and Fuller W. (1979). Distribution of the estimators for autoregressive time series with a unit root, *Journal of the American Statistical Association 74(366)*, 427-431.

Diebold F., and Mariano R. (1995). Comparing predictive accuracy, *Journal of Business & Economic Statistics 20(1)*, 253-263.

Enfield, D., Mestas-Nunez A., and Trimble, P. (2001). The Atlantic Multidecadal Oscillation and its relationship to rainfall and river flows in the continental U.S. *Geophysical Research Letters 28(10)*, 2077-2080.

Engle R., and Granger C. (1987). Co-integration and error correction: Representation, estimation and testing, *Econometrica 55(2)*, 251-276.

Engle, R., and Kozicki, S. (1993). Testing for common features. *Journal of Business & Economic Statistics 11(4)*, 369-395.

Estrada F., Gay-Garcia C., and Sánchez, A. (2010). Reply to "Does temperature contain a stochastic trend? Evaluating conflicting results by Kaufmann et al". *Climatic Change 101(3)*, 407-414.

Estrada, F., Martins, L., and Perron, P. (2017). Characterizing and attributing the warming trend in sea and land surface temperatures. *Atmósfera 30(2)*, 163-187.

Estrada, F., and Perron, P. (2014). Detection and attribution of climate change through econometric methods. *Boletín de la Sociedad Matemática Mexicana 20(1)*, 107-136.

Estrada, F., and Perron, P. (2017). Extracting and analyzing the warming trend in global and hemispheric temperatures. *Journal of Time Series Analysis 38(5)*, 711-732.

Estrada, F., and Perron, P. (2019). Causality from long-lived radiative forcings to the climate trend. *Annals of the New York Academy of Sciences 1436(1)*, 195-205.

Estrada F., Perron P., Gay-Garcia, C., and Martínez-López, B. (2013a). A time series analysis of the 20th century climate simulations produced for the IPCC's Fourth Assessment Report. *PloS one 8(3)*, e60017.

Estrada, F., Perron, P., and Martínez-López, B. (2013b). Statistically derived contributions of diverse human influences to twentieth-century temperature changes. *Nature Geoscience 6(12)*, 1050-1055.

Gay-Garcia C., Estrada F., and Sanchez A. (2009). Global and hemispheric temperature revisited. *Climatic Change 94(3-4)*, 333-349.

Gil-Alana, L. (2008). Time trend estimation with breaks in temperature time series. *Climatic Change 89(3-4)*, 325-337.

Hansen, J., and Lebedeff, S. (1987). Global trends of measured surface air temperature. *Journal of Geophysical Research: Atmospheres 92(D11)*, 13345-13372.

Hansen, J., Ruedy, R., Sato, M., and Lo, K. (2010). Global surface temperature change. *Reviews of Geophysics 48(4)*, RG4004.

Hansen J., Sato, M., Kharecha, P., and von Schuckmann, K. (2011). Earth's energy imbalance and implications. *Atmospheric Chemistry and Physics 11(24)*, 13421-13449.

Hansen, J. et al. (1996). A Pinatubo climate modeling investigation. In G. Fiocco, D. Fua, and G. Visconti (Eds.). *The Mount Pinatubo Eruption: Effects on the Atmosphere and Climate.* Springer, Berlin, Heidelberg, 233-272.

Houghton, J., Jenkins, G., and Ephraums, J. (1990). *Climate Change: The IPCC Scientific Assessment.* Cambridge University Press, Cambridge, U.K..

Hui, L., and Rodríguez, G. (2005). Human activities and climate change. A cointegration analysis. *Environmental Modelling and Software 20(6)*, 761-773.

Hurrell, J. (1995). Decadal trends in the North Atlantic Oscillation and relationships to regional temperature and precipitation. *Science 269(5224)*, 676-679.

Hurrell, J. (1996). Influence of variations in extratropical wintertime teleconnections on northern hemisphere temperature. *Geophysical Research Letters 23(6)*, 665-668.

IPCC-WGI. (2007). *Climate Change 2007: The Physical Science Basis.* Contribution of Working Group I to the Fourth Assessment Report of the Intergovernmental Panel on Climate Change. In S. Solomon, D. Qin, M. Manning, Z. Chen, M. Marquis, K.B. Averyt, M. Tignor and H.L. Miller (eds.). Cambridge University Press, Cambridge, United Kingdom and New York; and *Climate Change 2007: Impact, Adaptation and Vulnerability.* Contribution of the Working Group II to the Fourth Assessment Report of the Intergovernmental Panel on Climate Change. In M. Parry, O. Canziani, J. Palutikof, P. van der Linden and C. Hanson (Eds.). Cambridge University Press, Cambridge, United Kingdom and New York.

Jones, P., Raper, S., Bradley, R., Diaz, H., Kelly, P., and Wigley, T. (1986a). Northern hemisphere surface air temperature variations: 1851-1984. *Journal of Climate and Applied Meteorology 25(2)*,161-179.

Jones, P., Raper, S., and Wigley, T. (1986b). Southern hemisphere surface air temperature variations: 1851-1984. *Journal of Climate and Applied Meteorology 25(9)*,1213-1230.

Jones, P., Wigley, T., Wright, P. (1986c). Global temperature variations between 1861 and 1984. *Nature 322(6078)*, 430-434.

Kaufmann, R., Kauppi, H., and Stock, J. (2006a). Emissions, concentrations, & temperature: A time series analysis. *Climatic Change 77(3-4)*, 249-278.

Kaufmann, R., Kauppi, H., Stock, J. (2006b). The relationship between radiative forcing and temperature: What do statistical analyses of the instrumental temperature record measure? *Climatic Change 77(3-4)*, 279-289.

Kaufmann, R., and Stern, D. (1997). Evidence for human influence on climate from hemispheric temperature relations. *Nature 388(6637)*, 39-44.

Kerr, R. (2000). A North Atlantic climate pacemaker for the centuries. *Science 288(5473)*, 1984-1985.

Kim, D., and Perron P. (2009). Unit root tests allowing for a break in the trend function under both the null and the alternative hypotheses. *Journal of Econometrics 148(1)*, 1-13.

Knudsen, M., Seidenkrantz, M., Jacobsen, B., and Kuijpers, A. (2010). Tracking the Atlantic Multidecadal Oscillation through the last 8,000 years. *Nature Communications 2(178)*.

Knutti, R., and Hegerl, G. (2008). The equilibrium sensitivity of the Earth's temperature to radiation changes. *Nature Geoscience 1(11)*, 735-743.

Lehmann, E. (1975). *Nonparametrics: Statistical Methods Based on Ranks*. McGraw-Hill, San Francisco.

Mills, T. (2010a). 'Skinning a cat': alternative models of representing temperature trends. An editorial comment. *Climatic Change 101(3)*, 415-426.

Mills T. (2010b). Is global warming real? Analysis of structural time series models of global and hemispheric temperatures. *Journal of Cosmology 8*, 1947-1954.

Ng, S., and Perron, P. (2001). Lag length selection and the construction of unit root tests with good size and power. *Econometrica 69(6)*, 1519-1554.

Perron, P. (1989). The great crash, the oil price shock, and the unit root hypothesis. *Econometrica 57(6)*, 1361-1401.

Perron, P. (1997). Further evidence on breaking trend functions in macroeconomic variables. *Journal of Econometrics 80(2)*, 355-385.

Perron, P. (2006). Dealing with structural breaks. In T. Mills and K. Patterson (Eds.). *Palgrave Handbook of Econometrics, Vol. 1: Econometric Theory*. Palgrave Macmillan, New York, 278-352.

Perron, P., and Rodríguez, G. (2003). GLS detrending, efficient unit root tests and structural change. *Journal of Econometrics 115(1)*, 1-27.

Perron, P., and Vogelsang, T. (1993). Erratum: The great crash, the oil price shock and the unit root hypothesis, *Econometrica 61(1)*, 248-249.

Perron, P., and Yabu, T. (2009). Testing for shifts in trend with an integrated or stationary noise component. *Journal of Business & Economic Statistics 27(3)*, 369-396.

Perron, P., and Zhu, X. (2005). Structural breaks with deterministic and stochastic trends. *Journal of Econometrics 129(1-2)*, 65-119.

Said, E., and Dickey, D. (1984). Testing for unit roots in autoregressive moving average models of unknown order. *Biometrika 71(3)*, 599-607.

Saikkonen, P. (1991). Asymptotically efficient estimation of cointegration regressions. *Econometric theory 7(1)*, 1-21.

Schlesinger, M., and Ramankutty, N. (1994). An oscillation in the global climate system of period 65-70 years. *Nature 367(6465)*, 723-726.

Stern, D., and Kaufmann, R. (1997a). Is there a global warming signal in hemispheric temperature series? Working Papers in *Ecological Economics*, The Australian National University, Center for Resource and Environmental Studies Ecological Economics Programme.

Stern, D., and Kaufmann, R. (1997b). Time series properties of global climate variables: Detection and attribution of climate change. Working Paper in *Ecological Economics*, Australian National University, Center for Resource and Environmental Studies, Ecological Economics Programme.

Stock, J., and Watson, M. (1993). A simple estimator of cointegrating vectors in higher order integrated systems. *Econometrica 61(4)*, 783-820.

Tol, R., and De Vos, A. (1993). Greenhouse statistics - time series analysis. *Theoretical and Applied Climatology 48(2-3)*, 63-74.

Tol, R., and De Vos, A. (1998). A Bayesian statistical analysis of the enhanced greenhouse effect. *Climatic Change 38(1)*, 87-112.

Triacca, U. (2001). On the use of Granger causality to investigate the human influence on climate. *Theoretical and Applied Climatology 69(3-4)*, 137-138.

Vogelsang, T., and Perron, P. (1998). Additional tests for a unit root allowing the possibility of breaks in the trend function. *International Economic Review 39(4)*, 1073-1100.

Wigley, T., and Raper, S. (1990). Natural variability of the climate system and detection of the greenhouse effect. *Nature 344(6264)*, 324-327.

Wolter, K., and Timlin, M. (1998). Measuring the strength of ENSO - how does 1997/98 rank? *Weather 53(9)*, 315-324.

Zivot, E., and Andrews, D. (1992). Further evidence on the great crash, the oil-price shock, and the unit-root hypothesis. *Journal of Business and Economic Statistics 10(3)*, 25-44.